Microstructure, elevated-temperature mechanical properties and creep resistance of dispersoid-strengthened Al-Mn-Mg 3xxx alloys with varying Mg and Si contents

Zhen Li, Zhan Zhang, X.-Grant Chen *

Department of Applied Science, University of Quebec at Chicoutimi,
Saguenay, QC, Canada, G7H 2B1

Abstract

In the present work, the effects of magnesium and silicon addition on microstructure, elevated-temperature yield strength and creep resistance of Al-Mn-Mg 3xxx alloys were investigated. The microstructure evolution under as-cast and heat-treated conditions was quantitatively evaluated by optical and electron microscopy. Results revealed that both magnesium and silicon had an important influence on the distribution and volume fraction of precipitated dispersoids in 3xxx alloys. Without Mg or Si addition, dispersoids could hardly form during the precipitation heat treatment; hence, the alloys free of Mg or Si possessed low yield strength and creep resistance at elevated temperature. A significant improvement in elevated-temperature yield strength and creep resistance was obtained over a wide range of Mg (0.5-1.5 wt%) and Si (0.25-1 wt%) content studied due to the precipitation of a large number of dispersoids. The best combination of yield strength and creep resistance at 300 ℃ was obtained by the alloy containing 1.0 wt% Mg and 0.25 wt% Si with the maximum volume fraction of dispersoids and the minimum volume fraction of dispersoid free zone. The effects of dispersoid strengthening, solid solution strengthening and grain size on yield strength and creep resistance were discussed based on experimental results.

Keywords: Al-Mn-Mg 3xxx alloys; Mg addition; Si addition; Microstructure; Elevated-temperature mechanical properties; Creep resistance

* Corresponding author – X.-Gant Chen, Tel: (418) 545-5011 ext. 2603; Fax: (418) 545-5012; Email: xgrant.chen@uqac.ca

1. Introduction

At present, the growing demand for high performance and lightweight structural components at elevated temperatures (250 to 350 ℃) is a challenge for the weight-sensitive automotive and aerospace industries. The traditional precipitation-strengthened aluminum alloys such as 2xxx, 6xxx and 7xxx can hardly meet the requirements of elevated-temperature mechanical properties, because of the rapid coarsening of nano-scale precipitates at elevated temperatures (overaging effect) [1, 2]. In recent years, the dispersoid strengthening in 3xxx aluminum alloys that can improve the mechanical properties at both room and elevated temperatures has been discovered [3-7]. Although Al-Mn-Mg 3xxx alloys are traditionally classified as non-heat-treatable alloys, thermally stable α-Al(MnFe)Si dispersoids form during heat treatment and hence the improvement of high temperature properties in the 3004 alloy have recently been reported [5, 6]. In addition, Al-Mn-Mg 3xxx alloys possess good formability, excellent corrosion resistance and weldability [8, 9]. The combination of those properties makes 3xxx alloys especially attractive for elevated temperature applications.

Several studies have been conducted on the evolution of microstructure during different heat treatments in 3xxx alloys, focusing mainly on 3003 and 3004 alloys [3-6, 8, 10-19]. The as-cast microstructure of 3003 and 3004 alloys consists mainly of Al_6(MnFe), α-Al(MnFe)Si and Mg_2Si intermetallic phases [11, 16, 17, 20-22]. During heat treatment, the supersaturated solid solution decomposes and hence a number of α-Al(MnFe)Si dispersoids precipitate. The evolution of electrical conductivity is widely used to follow up the change of solute level during heat treatment, which gives a detailed indication of the precipitation of solute atoms from the supersaturated solid solution [8, 10]. In combination with the microhardness measurement, the precipitation kinetic of α-Al(MnFe)Si dispersoids and the corresponded peak precipitation condition can be determined [4, 5]. It is reported that the precipitation of α-Al(MnFe)Si dispersoids starts at approximately 340 °C and the maximum volume fraction can reach as high as ~3% [5]. The size and amount of dispersoids are dependent on the alloy chemistry and heat treatment conditions [3-5, 10, 18]. The α-Al(MnFe)Si dispersoids are partially coherent with the matrix [3, 23] and have a cubic crystal structure [10]. Interestingly,

the α-Al(MnFe)Si dispersoids are proven to be thermally stable at 300 ℃, resulting in excellent mechanical properties and creep resistance at elevated temperature [5].

To date, limited open literature is available concerning the effect of chemical composition on microstructure and elevated-temperature mechanical properties in Al-Mn-Mg 3xxx alloys. Muggerud et al [4] studied the effect of Mn and Si on the evolution of dispersoids in the 3003 alloy, and found that the addition of Mn and Si can promote the precipitation of α-Al(MnFe)Si dispersoids and thus improve room temperature mechanical properties. The effect of Fe on the dispersoid precipitation and elevated-temperature properties in 3004 alloy was investigated by Kun et al [6]. With an optimum Fe content, a high volume fraction of α-Al(MnFe)Si dispersoids form in the alloy and hence good mechanical properties and creep resistance at elevated temperature can be achieved.

In the present study, the effects of two main alloying elements in 3xxx alloys, Mg and Si, on the microstructure and elevated-temperature mechanical properties were investigated systematically. The microstructure evolution during heat treatment has been quantitatively evaluated by optical and electron microscopy. In addition, the creep properties at 300 ℃ as a function of Mg and Si content have been evaluated.

2. Experimental

Two series of experimental alloys with different Mg and Si contents were designed at the present work. In the first series (referred to as “DM” alloys), the Mg content changes from 0 to 2% while the Si content is fixed at 0.25%. In the second series (referred to as “DS” alloys), the Si content varies from 0 to 1% while the Mg content remains constant at 1%. In all of the experimental alloys, Mn and Fe were controlled at the same levels, approximately 1.25% and 0.6%, respectively. The chemical compositions as analyzed with the optical emission spectrometer are given in Table 1. All of the alloy compositions here are in wt% unless otherwise indicated.

The experimental alloys were prepared in an electric resistance furnace. The temperature of the melt was maintained at 750 ℃ for 30 min and then degassed for 15 min. The melt was

poured and solidified in a steel permanent mold preheated at 250 ℃. The dimension of the cast ingots was 30mm×40mm×80mm. To promote the precipitation of dispersoids, cast ingots were heat-treated at 375 ℃ with a heating rate of 5 ℃/min and then held for 24 hours, followed by water quench to room temperature. The heat treatment of 375℃/24h was used as the peak precipitation treatment in the previous work [6].

The compressive yield strength tests were conducted at 300 ℃ by a Gleeble 3800 thermomechanical simulator unit. The total strain of the deformed samples was 0.2 and the strain rate was 0.001 s^{-1}. The samples were machined in a cylinderical form with a 15 mm length and 10 mm diameter. The results were obtained from the average value of three tests. Creep tests were performed at 300 °C for 90 hours under the compression condition with a constant load of 45 MPa. Each condition was repeated three times. The sample size is the same as the Gleeble sample. Microhardness was evaluated by an NG-1000 CCD microhardness test machine with a load of 200 g and a 20-second holding time. The tests were performed on polished samples for at least 10 measurements. The samples for hardness tests and microstructure observation were prepared using conventionally metallographic polishing. The final polish step was completed with 1 μm diamond paste followed by 60 nm colloidal silica. Electrical conductivity was measured on the samples with machined surface by a Sigmascope SMP10 at room temperature, and at least 5 measurements were performed for each sample.

Optical microscopy was used to observe the distribution of the dispersoid zone and the dispersoid free zone (DFZ). To reveal the dispersoids, the samples were etched by 0.5% HF for 20 seconds. The image analysis with the software (Clemex PE 4.0) was used to quantify the amount of the intermetallics, the dispersoids zone and DFZ by color contrast. The volume fractions of the intermetallics, the dispersoids zone and DFZ were converted from the area fractions of the intermetallics, the dispersoids zone and DFZ measured by the image analysis from optical microscope images according to the Delesse's principle [24]. For each image analysis data, 100 graphs with x500 magnification were analyzed. A transmission electron microscope (TEM, JEM-2100) operated at 200kV was used to observe the morphology and

the size of the dispersoids. An electron energy loss spectroscope (EELS) attached to the TEM was used to measure the thickness of the samples. The size and number density of the dispersoids were quantified by the image analysis on the TEM images. The volume fraction of dispersoids was calculated using the method introduced in [10] shown in Eq. (1):

$$V_{\mathrm{v}} = A_{\mathrm{A}} \frac{\mathrm{K}\bar{\mathrm{D}}}{\mathrm{K}\bar{\mathrm{D}} + \mathrm{t}} (1 - A_{\mathrm{DFZ}}) \quad (1)$$

Where A_{A} is the volume fraction of dispersoids in TEM image, A_{DFZ} is the volume percentage of the DFZ, $\bar{D}$ is the average equivalent diameter of the dispersoids, t is the TEM foil thickness, and K is the average shape factor of dispersoids, which was taken to equal 0.45 in the present study.

3. Results

3.1 As-cast Microstructure

Fig. 1 shows the typical as-cast microstructure of the experimental alloys. The as-cast microstructure was generally composed of aluminum dendrite cells and a number of intermetallic phases, which distributed in the aluminum dendrite boundaries. In DM0 and DS0 alloys, there were only Mn-containing intermetallic particles ($Al_6(MnFe)$) in the interdendrite regions (Fig. 1a). With additions of Mg in the DM series and Si in the DS series, primary Mg_2Si appeared in the as-cast microstructure. Under the optical microscope (Fig. 1), the primary Mg_2Si particles are in dark color while $Al_6(MnFe)$ intermetallics appear in grey color. As the content of Si increased, a small number of α-Al(MnFe)Si intermetallic particles are also observed but they are not specifically distinguished due to their similarity with $Al_6(MnFe)$ intermetallics. Two different intermetallic phases co-existed in aluminum dendrite boundaries: Mn-containing intermetallic particles as a major phase and primary Mg_2Si particles as a minor phase (Fig. 1b). The microstructural features of Mg-containing DM series (DM50, 100, 150, 200 alloys) and Si-containing DS series (DS25, 45, 70, 100 alloys) are very similar, but the amounts of intermetallic phases change with alloying element content. The volume fractions of both intermetallic phases in DM and DS series alloys were

quantified by image analysis, as shown in Fig. 2 (a) and (b). With increasing Mg and Si contents, the volume fraction of Mn-containing intermetallic particles increases moderately while the amount of primary Mg_2Si particles increases rapidly.

3.2 Microstructure after heat treatment

3.2.1 Dispersoid and dispersoid free zones

After heat-treatment at 375℃/24h, a number of α-Al(MnFe)Si dispersoids precipitated in the aluminum matrix of both DM and DS series. By etching with 0.5% HF, the precipitated dispersoids can be clearly revealed. In optical images, the dispersoid zone and dispersoid free zone (DFZ) are visible as shown in Fig. 3 and Fig. 4. The dispersoid zone is an area with a high number density of α-Al(MnFe)Si dispersoids, while the DFZ is the area with very few α-Al(MnFe)Si dispersoids present. The volume fractions of the dispersoid zone and DFZ were analyzed by the image analysis, and the results are shown in Fig. 5. For the DM0 alloy (0%Mg), only a few of dispersoids appeared around intermetallic particles, which left an extensive DFZ in the microstructure, as shown in Fig. 3a. The percentage of the dispersoid zone was only approximately 20%. With increasing Mg to 0.5% Mg (DM50 alloy), a larger number of dispersoids appeared (Fig. 3b) and the dispersoid zone increased to ~45% (Fig. 5). When 1.0% Mg was added (DM100 alloy), the precipitated dispersoids continued to increase (Fig. 3c), and the percentage of the dispersoid zone reached the maximum value of ~70%. With Mg content increasing further in DM150 and DM200 alloys, the percentage of the dispersoid zone decreased slightly while the DFZ increased moderately, and both values remained more or less stable (Figs. 3d and 5).

In the DS series, the precipitation of dispersoids depends largely on Si content. In the base alloy (DS0 alloy with 0% Si), very few dispersoids can be observed and no clear dispersoid zone can be defined in the microstructure (Fig. 4a). Without Si addition, the dispersoids can hardly form during heat treatment. With 0.23% Si addition (DS25 alloy), a large number of dispersoids appear (Fig. 4b) and the volume fraction of the dispersoid zone reaches to ~70% (Fig. 5). By increasing the Si to 0.42% (DS45 alloy), a dense distribution of

dispersoids remains in the microstructure (Fig. 4c), and the volume fraction of the dispersoid zone decreases slightly to ~50%. By increasing the Si further to 0.7% and more (DS70 and DS100 alloys), in addition to the dispersoid precipitation, a number of coarse β-Mg_2Si particles (black needle phase in the optical microstructure) appear, accompanied by large DFZs (Fig. 4d). Apparently, the high levels of Si and Mg in DS70 and DS100 alloys induced the precipitation of coarse β-Mg_2Si particles, which consumed a large amount of the Si solutes in the matrix, and those Si atoms were no longer available for the formation of dispersoids. Consequently, the volume fraction of the dispersoid zone in DS70 and DS100 samples decreases while the volume fraction of DFZ continues to increase (Fig. 5).

3.2.2 Precipitation of dispersoids in aluminum matrix

Due to the submicron size of the dispersoids, the precipitation of dispersoids in the dispersoid zone was closely observed by TEM. Typical TEM images in the DM and DS series are shown in Figs. 6 and 7. All of the TEM images were taken along the <001> axis direction of Al. The size and number density of dispersoids were quantified by the image analysis on TEM images, and the results are shown in Fig. 8. In general, the dispersoids have two morphologies: cubic-shaped and plate-shaped, as shown in Fig. 6a. Using TEM-EDS, no significant difference in the composition was found between these two morphologies. All dispersoids have a composition close to $Al_{12\text{-}20}(MnFe)_3Si$, which is referred to as α-Al(MnFe)Si dispersoids in the present work, according to the literature [5, 10].

In the DM0 alloy without Mg, the dispersoids distributes sparsely after heat-treatment at 375℃/24h (Fig. 6a). The size of the dispersoids is quite large (in the range of 100 nm) and the number density is very low (Fig. 8). With Mg addition, the precipitation of dispersoids is largely promoted (Figs. 6b and c). The size of the dispersoids in the DM50 alloy decreases to ~45 nm, and the number density increases greatly to 1500/μm^3, which reaches the peak value in the DM series. With further increasing Mg content, the size of the dispersoids increases slightly and remains nearly constant at the value of ~50 nm, while the number density of the dispersoids decreases moderately with an increase in Mg content (Fig. 8).

In the DS0 alloy without Si, very few dispersoids can be observed in the aluminum matrix and most of them have precipitated along dislocations (Fig. 7a). With the addition Si at 0.23 – 0.7% in DS25, DS45 and DS70 alloys, a great number of dispersoids were present in the aluminum matrix (Fig. 7b). The size of the dispersoids ranges from 40 to 50 nm and the number density lies in the range of 1500/μm^3 (Fig. 8). The alloy with the highest Si (DS100) has the smallest dispersoids and the densest dispersoids in the dispersoid zone as shown in Fig.7 (c), although it exhibits a high percentage of DFZ (Fig. 5).

The volume fractions of dispersoids in all of the alloys were calculated according to Eq. 1, and the results are presented in Fig. 9. The tendency of volume fraction with alloying element content is similar in two series of alloys. In both base alloys (DM0 and DS0), the volume fractions of dispersoids are very low because of lack of Mg or Si. In the DM series when the Mg content increases to 1% (DM100), the volume fraction of dispersoids reaches its peak value, while the maximum volume fraction of dispersoids is obtained in the DS25 alloy with 0.23% Si in the DS series. Since the DM 100 and DS25 alloys have a similar chemical composition, the results from both the DM and DS series indicate that the alloy with 1.0% Mg and 0.25% Si has the maximum volume fraction of dispersoids (~2.75 vol.%) and the minimum DFZ. As the Mg content is over 1% in the DM series and the Si content is above 0.23% in the DS series, the volume fractions of dispersoids decrease with increasing alloying elements, primarily due to the increase of DFZs in the microstructure (Fig. 5).

3.3 Electrical conductivity and microhardness

To study the precipitation behavior of dispersoids, the evolution of electrical conductivity (EC) and microhardness as a function of holding time at 375 ℃ was determined experimentally. The results of EC and microhardness in the DM series are shown in Fig. 10. The EC in all of the alloy samples increases rapidly in the first several hours and then gradually rises to reach a plateau after 24 h. For the DM0 alloy, the increase of EC is mainly due to the decrease in the supersaturated Mn level in the aluminum matrix, which results from the precipitation of a limited number of α-Al(MnFe)Si dispersoids (Fig. 3a) and

a slight increase in the amount of intermetallic particles during heat treatment [11]. For all other Mg-containing alloys, the increase of EC with time is caused by the continuous decomposition of the supersaturated solid solution (Mn and Si) and the precipitation of a large amount of α-Al(MnFe)Si dispersoids (Fig. 3b-d).

Except the DM0 alloy, the microhardness of four other alloys increases with increasing holding time (Fig. 10b), indicating the strengthening effect of dispersoids that is confirmed by the microstructure observation (Fig. 3b-d). The values of microhardness reach the maximum level after 24 h holding time and become quite stable up to 48 h holding time, indicating that the full precipitation of dispersoids was achieved mostly after 24 h holding. For the base alloy without Mg (DM0), the microhardness drops slightly with the increase in the holding time, because a limited precipitation of dispersoids has little strengthening effect and the reduction of the Mn solute level with holding time leads to a weak matrix.

At any given holding time, the EC decreases and the microharness increases with increasing Mg content in the DM series, suggesting that in addition to the dispersoid precipitation, the alloying element in the solid solution also plays an important role in EC and microhardness. During the heat treatment of four Mg-containing alloys, the most Mn and Si were consumed due to the precipitation process of α-Al(MnFe)Si dispersoids. However, almost no Mg-containing phases formed after heat treatment. Therefore, it is reasonable to assume that except for the Mg bonded in primary Mg_2Si particles, almost all Mg solutes remained in aluminum matrix. The upper limit values of Mg and Si concentrations in the solid solution after heat treatment can be calculated, as shown in Table 2. Evidently, a considerable amount of Mg remained in the solid solution of four Mg-containing alloys, and the Mg solute level increased with increasing Mg addition, which causes the reduced EC and increased microhardness in the DM series.

The EC and microhardness as a function of holding time in the DS series are shown in Fig. 11. In the base alloy (DS0), the EC increases only slightly with holding time, indicating an insignificant precipitation of dispersoids (Fig. 4a). In all other Si-containing alloys, the values of EC increase remarkably with holding time, suggesting a strong dispersoid

precipitation during heat treatment. Because of lack of a strengthening phase, the microhardness of the DS0 alloy remains almost unchanged during holding time, and its values are generally lower than the microhardness values of other Si-containing alloys. With precipitation of α-Al(MnFe)Si dispersoids (Fig. 4b), the microhardness of the DS25 and DS45 alloys increases with holding time and reaches a plateau after 24 h holding. In the case of high Si alloys (DS70 and DS100), the values of microhardness after 24 h holding are lower than those of DS25 and DS45 alloys, which is attributed to the reduced dispersoid precipitation and the presence of coarse β-Mg_2Si precipitates (Fig. 4c-d).

3.4 Yield strength at 300 ℃

The elevated-temperature yield strengths of the DM and DS series are shown in Fig. 12. In the DM series, the DM0 alloy with 0% Mg possesses the lowest yield strength (43 MPa at 300 ℃). With 0.47% Mg in the DM50 alloy, the yield strength increases sharply to 75 MPa. With increasing Mg content to 1% (DM100), the yield strength continues to increase and reaches 80 MPa. A further increase of Mg up to 2% does not bring additional benefit and the yield strength remains at a similar level.

The large increase of yield strength up to 1% Mg can be attributed mainly to the increase in the dispersoid volume fraction. The volume fraction of dispersoids increases from 0.3% in the DM0 alloy to 1.6% in the DM50 alloy and further to 2.75% in the DM100 alloy (Fig. 9). When Mg increases from 1% to 2%, the volume fraction of dispersoids decreases from its maximum level of 2.75% in the DM100 alloy to 1.6-1.8% in the DM150 and DM200 alloys, which could result in a reduction of yield strength. However, the Mg solute level increases from 0.89% (DM100) to 1.36% (DM150) and further to 1.88% (DM200), as shown in Table 2. It is most likely that the increased solid solution strengthening of Mg could compensate for the reduced dispersoid strengthening in the DM150 and DM200 alloys. Therefore, the yield strength in three alloys (DM100, DM150 and DM200) remains at a similar level.

In the DS series, the DS0 alloy with 0% Si has a relatively low value for the yield strength (60 MPa at 300 ℃). With 0.23% Si addition in the DS25 alloy, the yield strength

increases remarkably to 80 MPa. With further increase of the Si up to 1%, the yield strength decreases moderately and remains at a similar level of 72-75 MPa for the DS45, DS70 and DS100 alloys.

Compared to the DM0 alloy, the DS0 alloy has considerably higher yield strength (Fig. 12). Both base alloys have an insufficient dispersoid precipitation, leading to a negligible dispersoid strengthening. However, the DS0 alloy contains 1% Mg, which is almost in the solid solution and provides the Mg solid solution strengthening. However, all alloys in the DS series have the same Mg content and hence, the effect of the Mg solid solution on yield strength is more or less the same. Therefore, the yield strength in the DS series is closely related to the volume fraction of dispersoids. For instance, the yield strength of DS25 alloy is 20 MPa higher than that of the DS0 alloy, attributed to the α-Al(MnFe)Si dispersoid strengthening. The moderate decrease in yield strength for the high Si alloys (0.45 to 1%) is caused mainly by the reduced volume fraction of dispersoids (Fig. 9).

3.5 Creep resistance at 300 ℃

Creep properties are considered one of most important material properties for high temperature applications. The compressive creep tests were conducted at 300 ℃ under a constant load of 45 MPa. The typical creep curves are shown in Fig. 13. It is obvious that after the creep tests, both the DM0 and DS0 alloys have the highest creep deformation, followed by the DM200 and DM150 alloys, while the other alloys (DM50, DM100, DS25, DS45, DS70 and DS100 alloys) show very little creep deformation at 300 ℃. During compressive creep deformation, the creep strain increases rapidly in the first few hours. After this initial stage, the creep deformation turns to a quasi-steady state, in which the creep rate becomes more or less constant with the progress of the creep deformation. The minimum creep rate can be calculated as the average creep rate in the quasi-steady state. In the present work, the total creep strain and the minimum creep rate are used to characterize the creep properties. The smaller the total creep strain and minimum creep rate, the better the creep

resistance is. The results of the total strain and minimum creep rate of all tested samples are shown in Fig. 14.

Two base alloys (DM0 and DS0) have the highest total strain and minimum creep rate, indicating the lowest creep resistance in the DM and DS series. Both alloys have an insufficient number of dispersoids, acting as barriers to the movement of dislocations and grain boundaries. However, the DS0 alloy has higher creep resistance that the DM0 alloy due to 1% Mg solutes in the matrix, which can also impede dislocation movement and decrease the grain boundary mobility. In the DM series, the total strain and minimum creep rate decrease sharply to the lowest level in the DM50 and DM100 alloys, indicating a significant improvement in the creep resistance attributed mainly to the increased amount of dispersoids and partially to a higher Mg solute relative to the DM0 alloy. During creep deformation, a large number of dispersoids present act as strong barriers impeding the dislocation movement, which is confirmed by TEM examination after the creep test in DM100 alloy that contained the highest dispersoid volume fraction in DM series (Fig. 15). In the DS series, the total strain and minimum creep rate drop from the highest level in the DS0 alloy to the lowest level in the DS25 alloys, showing a great gain in the creep resistance. With a further increase in the Si content, the creep resistance of the DS45, DS70 and DS100 alloys remains almost unchanged.

The evolution of creep resistance in the DM series is somewhat different from the tendency of the yield strength, especially with high Mg-containing alloys (DM150 and DM200), suggesting that there is another factor affecting the creep resistance. The creep resistance at high temperatures is reported to be sensitive to the grain size of the materials [25, 26]. Creep deformation can occur by grain boundary sliding and vacancy diffusions through the grain boundary, especially at high temperatures. The finer the grain size and thus more grain boundary area, the more easily the creep deformation occurs. The grain sizes of experimental alloys have been examined and measured by the electron backscatter diffraction technique (EBSD). The results are listed in Table 3 and typical grain structures of two alloys, DM200 and DM50, are shown in Fig. 16. DM200 and DM50 alloys contain the maximum

and minimum magnesium concentration respectively in the magnesium contained alloys. With the increase in Mg content, the average grain size in the DM series decreases. It would be contributed to the increase of the constitutional undercooling at the front of the solid/liquid interface during solidification by Mg addition [27]. The negative effect of grain size on the creep resistance in the DM50 and DM 100 alloys can be overlapped by the large amount of dispersoids. However, the grain size decreases significantly in the DM150 and DM200 alloys, which is believed to be the main reason that the creep resistance deteriorates. In the DS series, the grain sizes of all alloys are almost the same, which is close to the grain sizes of the DM50 and DM100 alloys. In addition, the total strain and minimum strain rate of the DS25, DS45, DS70 and DS 100 alloys are very close to those of the DM50 and DM100 alloys. Therefore, the gain size is not an additional factor influencing the creep resistance in the DS series.

4. Discussion

It is evident that Mg and Si contents in the 3xxx alloys have a strong influence on the microstructure and elevated-temperature mechanical properties. The results in the DM alloy series demonstrated that without Mg addition (DM0 alloy), the precipitation of dispersoids was so difficult that only an insufficient number of dispersoids came out. With Mg addition, a large number of α-Al(MnFe)Si dispersoids precipitated and the volume fraction of dispersoids increased significantly, indicating the important role of Mg in promoting the dispersoid precipitation. In Mn-containing Al-Mg-Si alloys [28, 29], the pre-existing β'-Mg_2Si is reported to be the prerequisite for a high density nucleation of α-Al(MnFe)Si dispersoids. In the present work, we observed that, during the heating process towards 375 ℃, a large number of β'-Mg_2Si precipitated at the temperature range of 200-300 ℃ and then slowly dissolved at higher temperatures of 300-375 ℃. Fig. 17a shows a TEM image of the water-quenched DM100 sample during heating at 275 ℃, in which lath-shaped β'-Mg_2Si precipitated and aligned along $<100>_{Al}$ in the matrix. When the temperature rose to 375℃ and during further holding, most of β'-Mg_2Si dissolved and α-Al(MnFe)Si preferentially nucleated and grew in the original area and orientation where pre-existing β'-Mg_2Si was (Fig.

17b). Due to the lack of Mg in the DM0 alloy, no pre-existing β'-Mg_2Si could be found during the heating process. Therefore, it is reasonable to believe that a proper Mg content provide an essential condition for precipitation of β'-Mg_2Si before the formation of α-Al(MnFe)Si dispersoids, which strongly promotes the nucleation of α-Al(MnFe)Si dispersoids during heat treatment.

Si is the essential element for α-Al(MnFe)Si dispersoids formation. Without Si (DS0 alloy), α-Al(MnFe)Si dispersoids can hardly form even after prolonged heat treatment because of lack of Si atoms in the matrix. With Si addition accompanied by 1%Mg in the DS series, a large number of dispersoids precipitated due to the same promoting effect of pre-existing β'-Mg_2Si on the nucleation of α-Al(MnFe)Si dispersoids, resulting in a significant improvement of YS and creep resistance at 300 ℃ in all Si-containing alloys in the DS series. With Si addition at 0.23% (DS25 alloy), it seems that an optimum combination of Mg and Si arrives, leading to the highest volume of dispersoids and hence the highest values of YS and creep resistance. In fact, the DM100 and the DS25 alloys have almost the same chemical composition (Table 1). The results from both the DM and DS series confirm that the alloy containing 1% Mg and 0.25% Si attains the best level of elevated-temperature strength and creep resistance.

It has been demonstrated that once precipitated, α-Al(MnFe)Si dispersoids are thermally stable at 300 ℃ [5], which is specially suitable as a strengthening phase in the aluminum matrix for high temperature applications. Compared to both base alloys (DM0 and DS0), all of the alloys containing Mg and Si in the DM and DS series show better precipitation of dispersoids and hence, remarkably higher YS and creep resistance at 300 ℃, confirming the important role of dispersoid strengthening at elevated temperatures. Furthermore, the DM100 and DS25 alloys have the same Mg content as the DS0 alloy but achieves the highest YS and creep resistance at 300 ℃ with the maximum volume fraction of dispersoids, clearly indicating the strong dispersoid strengthening effect. On the other hand, because pre-existing β'-Mg_2Si dissolved back into the matrix and no further Mg-containing phases formed during the heat treatment, the solute Mg in the matrix can provide an additional strengthening effect

on the elevated-temperature mechanical properties. When the Mg content is above 1%, the promotion effect on α-Al(MnFe)Si dispersoids seems to become weaker, and the volume fraction of dispersoids decreases moderately. However, the increase in the solute Mg level with the increasing Mg content in the alloys (Table 2) can compensate for the reduced dispersoid strengthening. Therefore, YS at 300 ℃ in the higher Mg-containing alloys can maintain a level similar to the DM100 alloy. It becomes evident that the increase in elevated-temperature strength and creep resistance in the experimental alloys studied is the synthetic effect of dispersoid strengthening and Mg solid solution strengthening, in which the precipitation of α-Al(MnFe)Si dispersoids plays the dominant role in the strengthening mechanism.

In addition to the best performance of the alloy containing 1% Mg and 0.25%Si, a significant improvement in overall elevated-temperature yield strength and creep resistance was achieved for the alloys with a wide range of Mg (0.5-1.5%) and Si (0.25-1.0%) (Figs. 12 and 14), providing great flexibility in the alloy design and selection for developing high-temperature resistant aluminum alloys.

5. Conclusions

1. Mg and Si have a significant influence on the distribution and volume fraction of dispersoids in Al-Mn-Mg 3xxx alloys. Without Mg or Si addition, α-Al(MnFe)Si dispersoids could hardly form during the precipitation heat treatment.
2. Mg and Si strongly promote the formation of α-Al(MnFe)Si dispersoids during precipitation heat treatment at 375 ℃. With 1% Mg and 0.25% Si, the alloy obtained the maximum volume fraction of dispersoids and the minimum volume fraction of the dispersoid free zone. Further increase of Mg and Si content resulted in a reduced volume fraction of dispersoids.
3. The base alloy free of Mg or Si possessed low yield strength and creep resistance at elevated temperature due to the lack of the strengthening phases. A significant improvement in yield strength and creep resistance at 300 ℃ was obtained over a wide range of Mg (0.5-1.5%) and Si (0.25-1.0%) contents studied, confirming the important strengthening effect of thermally stable dispersoids at elevated temperature.
4. The alloy containing 1.0% Mg and 0.25% Si demonstrated the best overall performance in terms of the distribution and volume fraction of dispersoids, elevated-temperature yield strength and creep resistance.

Acknowledgments

The authors would like to acknowledge the financial support of the Natural Sciences and Engineering Research Council of Canada (NSERC) and Rio Tinto Aluminum through the NSERC Industry Research Chair in the Metallurgy of Aluminum Transformation at University of Quebec at Chicoutimi.

References

1. I. J. Polmear, M. J. Couper, Design and development of an experimental wrought aluminum alloy for use at elevated temperatures, Metallurgical Transactions A. 19 (1988) 1027-1035. Doi: http://dx.doi.org/10.1007/BF02628387.
2. Y. Zhou, Z. Liu, S. Bai, P. Ying, L. Lin, Effect of Ag additions on the lengthening rate of Ω plates and formation of σ phase in Al-Cu-Mg alloys during thermal exposure, Materials Characterization. 123 (2017) 1-8. Doi: http://dx.doi.org/10.1016/j.matchar.2016.11.008.
3. Y. J. Li, A. M. F. Muggerud, A. Olsen, T. Furu, Precipitation of partially coherent α-Al(Mn,Fe)Si dispersoids and their strengthening effect in AA 3003 alloy, Acta Materialia. 60 (2012) 1004-1014. Doi: http://dx.doi.org/10.1016/j.actamat.2011.11.003.
4. A. M. F. Muggerud, E. A. Mørtsell, Y. Li, R. Holmestad, Dispersoid strengthening in AA3xxx alloys with varying Mn and Si content during annealing at low temperatures, Materials Science and Engineering: A. 567 (2013) 21-28. Doi: http://dx.doi.org/10.1016/j.msea.2013.01.004.
5. K. Liu, X. G. Chen, Development of Al–Mn–Mg 3004 alloy for applications at elevated temperature via dispersoid strengthening, Materials & Design. 84 (2015) 340-350. Doi: http://dx.doi.org/10.1016/j.matdes.2015.06.140.
6. K. Liu, X.-G. Chen, Evolution of Intermetallics, Dispersoids, and Elevated Temperature Properties at Various Fe Contents in Al-Mn-Mg 3004 Alloys, Metallurgical and Materials Transactions B. 47 (2016) 3291-3300. Doi: http://dx.doi.org/10.1007/s11663-015-0564-y.
7. K. Liu, H. Ma, X. G. Chen, Enhanced elevated-temperature properties via Mo addition in Al-Mn-Mg 3004 alloy, Journal of Alloys and Compounds. 694 (2017) 354-365. Doi: http://dx.doi.org/10.1016/j.jallcom.2016.10.005.
8. H.-W. Huang, B.-L. Ou, Evolution of precipitation during different homogenization treatments in a 3003 aluminum alloy, Materials & Design. 30 (2009) 2685-2692. Doi: http://dx.doi.org/10.1016/j.matdes.2008.10.012.
9. A. R. Yazdzad, T. Shahrabi, M. G. Hosseini, Inhibition of 3003 aluminum alloy corrosion by propargyl alcohol and tartrate ion and their synergistic effects in 0.5% NaCl solution, Materials Chemistry and Physics. 109 (2008) 199-205. Doi: http://dx.doi.org/10.1016/j.matchemphys.2007.11.012.
10. Y. J. Li, L. Arnberg, Quantitative study on the precipitation behavior of dispersoids in DC-cast AA3003 alloy during heating and homogenization, Acta Materialia. 51 (2003) 3415-3428. Doi: http://dx.doi.org/10.1016/S1359-6454(03)00160-5.
11. Y. J. Li, L. Arnberg, Evolution of eutectic intermetallic particles in DC-cast AA3003 alloy during heating and homogenization, Materials Science and Engineering: A. 347 (2003) 130-135. Doi: http://dx.doi.org/10.1016/S0921-5093(02)00555-5.
12. Q. Du, W. J. Poole, M. A. Wells, N. C. Parson, Microstructure evolution during homogenization of Al–Mn–Fe–Si alloys: Modeling and experimental results, Acta Materialia. 61 (2013) 4961-4973. Doi:

http://dx.doi.org/10.1016/j.actamat.2013.04.050.
13. Q. Zhao, B. Holmedal, Y. Li, Influence of dispersoids on microstructure evolution and work hardening of aluminium alloys during tension and cold rolling, Philosophical Magazine. 93 (2013) 2995-3011. Doi: http://dx.doi.org/10.1080/14786435.2013.794315.
14. A. M. F. Muggerud, Y. Li, R. Holmestad, Composition and orientation relationships of constituent particles in 3xxx aluminum alloys, Philosophical Magazine. 94 (2014) 556-568. Doi: http://dx.doi.org/10.1080/14786435.2013.857796.
15. N. Sun, B. R. Patterson, J. P. Suni, E. A. Simielli, H. Weiland, L. F. Allard, Microstructural evolution in twin roll cast AA3105 during homogenization, Materials Science and Engineering: A. 416 (2006) 232-239. Doi: http://dx.doi.org/10.1016/j.msea.2005.10.018.
16. M. Dehmas, E. Aeby-Gautier, P. Archambault, M. Serrière, Interaction Between Eutectic Intermetallic Particles and Dispersoids in the 3003 Aluminum Alloy During Homogenization Treatments, Metallurgical and Materials Transactions A. 44 (2013) 1059-1073. Doi: http://dx.doi.org/10.1007/s11661-012-1473-1.
17. Z. Li, Z. Zhang, X. G. Chen, Effect of magnesium on dispersoid strengthening of Al—Mn—Mg—Si (3xxx) alloys, Transactions of Nonferrous Metals Society of China. 26 (2016) 2793-2799. Doi: http://dx.doi.org/10.1016/S1003-6326(16)64407-2.
18. S. P. Chen, N. C. W. Kuijpers, S. van der Zwaag, Effect of microsegregation and dislocations on the nucleation kinetics of precipitation in aluminium alloy AA3003, Materials Science and Engineering: A. 341 (2003) 296-306. Doi: http://dx.doi.org/10.1016/S0921-5093(02)00245-9.
19. M. Dehmas, P. Weisbecker, G. Geandier, P. Archambault, E. Aeby-Gautier, Experimental study of phase transformations in 3003 aluminium alloys during heating by in situ high energy X-ray synchrotron radiation, Journal of Alloys and Compounds. 400 (2005) 116-124. Doi: http://dx.doi.org/10.1016/j.jallcom.2005.03.062.
20. M. Warmuzek, G. Mrówka, J. Sieniawski, Influence of the heat treatment on the precipitation of the intermetallic phases in commercial AlMn1FeSi alloy, Journal of Materials Processing Technology. 157–158 (2004) 624-632. Doi: http://dx.doi.org/10.1016/j.jmatprotec.2004.07.125.
21. D. T. L. Alexander, A. L. Greer, Solid-state intermetallic phase tranformations in 3XXX aluminium alloys, Acta Materialia. 50 (2002) 2571-2583. Doi: http://dx.doi.org/10.1016/S1359-6454(02)00085-X.
22. H. D. Merchant, J. G. Morris, D. S. Hodgson, Characterization of intermetallics in aluminum alloy 3004, Materials Characterization. 25 (1990) 339-373. Doi: http://dx.doi.org/10.1016/1044-5803(90)90062-O.
23. A. M. F. Muggerud, J. C. Walmsley, R. Holmestad, Y. Li, Combining HAADF STEM tomography and electron diffraction for studies of α-Al(Fe,Mn)Si dispersoids in 3xxx aluminium alloys, Philosophical Magazine. 95 (2015) 744-758. Doi: http://dx.doi.org/10.1080/14786435.2015.1006294.
24. G. F. V. Voort, ASM Handbook: Metallography and Microstructures. (ASM

International, 2004), Vol. 9, pp. 429.
25. R. L. Coble, A Model for Boundary Diffusion Controlled Creep in Polycrystalline Materials, Journal of Applied Physics. 34 (1963) 1679-1682. Doi: http://aip.scitation.org/doi/abs/10.1063/1.1702656.
26. C. Herring, Diffusional Viscosity of a Polycrystalline Solid, Journal of Applied Physics. 21 (1950) 437-445. Doi: http://aip.scitation.org/doi/abs/10.1063/1.1699681.
27. Y. Birol, Effect of solute Mg on grain size of aluminium alloys, Materials Science and Technology. 28 (2012) 924-927. Doi: http://dx.doi.org/10.1179/1743284712Y.0000000024.
28. L. Lodgaard, N. Ryum, Precipitation of dispersoids containing Mn and/or Cr in Al–Mg–Si alloys, Materials Science and Engineering: A. 283 (2000) 144-152. Doi: http://dx.doi.org/10.1016/S0921-5093(00)00734-6.
29. H. Hirasawa, Precipitation process of Al-Mn and Al-Cr supersaturated solid solution in presence of age hardening phases, Scripta Metallurgica. 9 (1975) 955-958. Doi: http://dx.doi.org/10.1016/0036-9748(75)90551-7.

Tables

Table 1 Chemical compositions of the experimental alloys investigated (wt%)

Alloy ID	Mg	Si	Fe	Mn	Al
DM0	**0**	0.25	0.60	1.20	Bal.
DM50	**0.47**	0.25	0.56	1.24	Bal.
DM100 *	**1.00**	0.25	0.60	1.24	Bal.
DM150	**1.50**	0.26	0.60	1.24	Bal.
DM200	**2.02**	0.27	0.60	1.24	Bal.
DS0	1.02	**0.03**	0.56	1.25	Bal.
DS25 *	1.05	**0.23**	0.53	1.25	Bal.
DS45	1.07	**0.42**	0.57	1.26	Bal.
DS70	1.01	**0.70**	0.54	1.25	Bal.
DS100	1.00	**0.97**	0.56	1.28	Bal.

* With cross change of Mg and Si content in both DM and DS series, the chemical compositions of the DM100 alloy and the DS25 alloy are similar.

Table 2 Estimated Mg and Si contents in the solid solution after heat-treatment at 375℃/24h

ID	Original content (wt%)		Volume fraction of primary Mg_2Si (%)	Bonded in primary Mg_2Si (wt%)		Upper bound content in solid solution (wt%)	
	Mg	Si		Mg	Si	Mg	Si
DM0	0	0.25	0	0	0	0	0.25
DM50	0.47	0.25	0.10	0.05	0.03	0.42	0
DM100	1.00	0.25	0.24	0.11	0.06	0.89	0
DM150	1.50	0.26	0.30	0.14	0.08	1.36	0
DM200	2.02	0.27	0.30	0.14	0.08	1.88	0

Table 3 Grain size of different alloys in as-cast condition

	DM0	DM50	DM100	DM150	DM200	DS25	DS45	DS70	DS100
Equivalent grain diameter (μm)	775	539	556	342	302	512	495	459	523

Figures

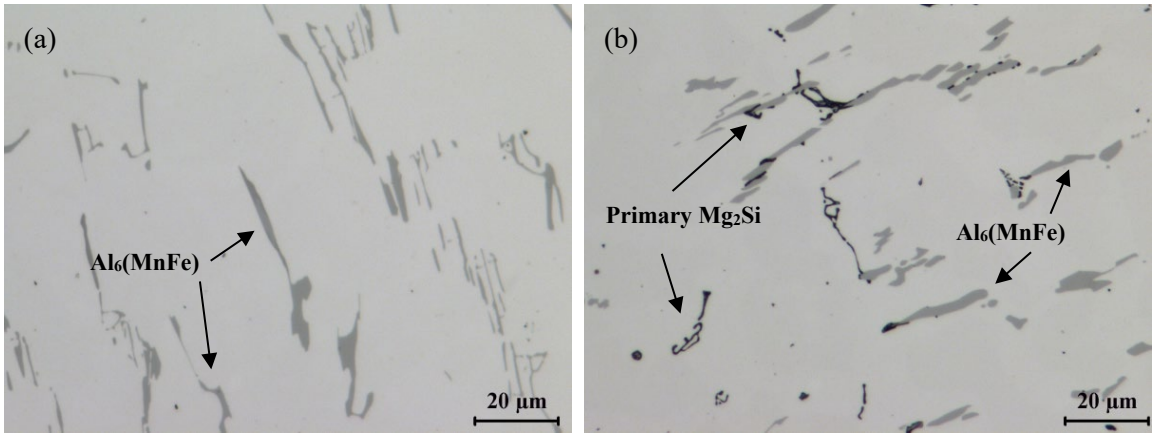

Fig.1 As-cast microstructure of (a) DM0 alloys (0% Mg) and (b) DM100 alloys (1.0% Mg).

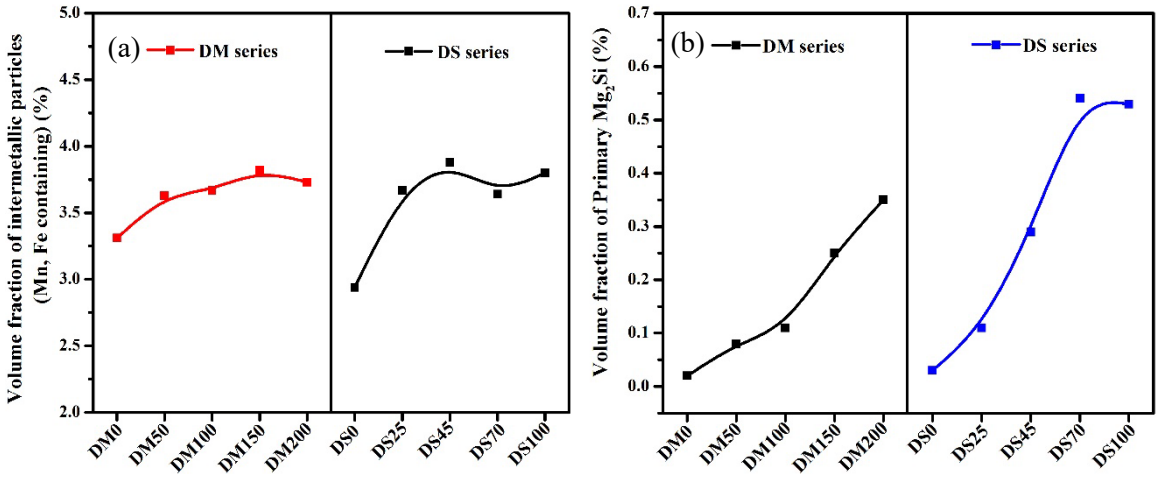

Fig. 2 Volume fraction of Mn-, Fe-containing intermetallic particles (a) and primary Mg_2Si particles (b) of the as-cast samples.

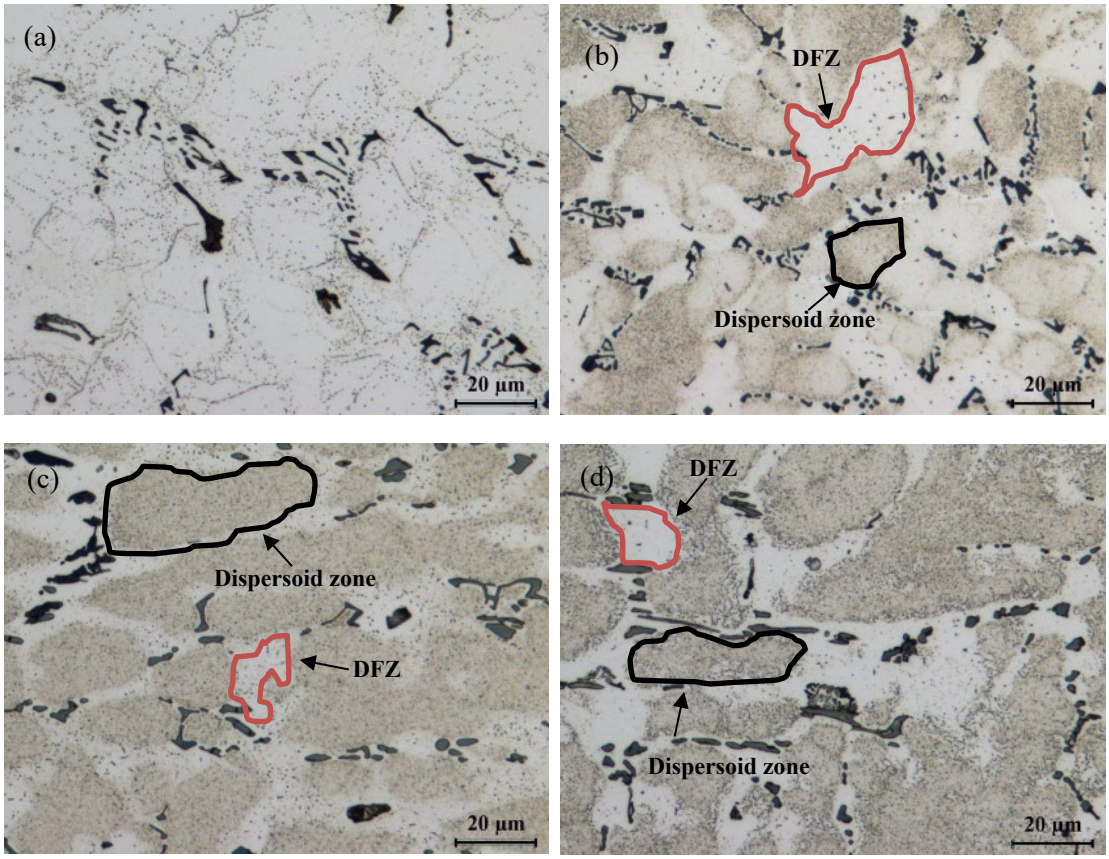

Fig. 3 Distribution of the dispersoid zone and DFZ in the DM series (a) DM0 alloy (0% Mg), (b) DM50 alloy (0.47%% Mg), (c) DM100 alloy (1.00% Mg) and (d) DM200 alloy (2.02% Mg).

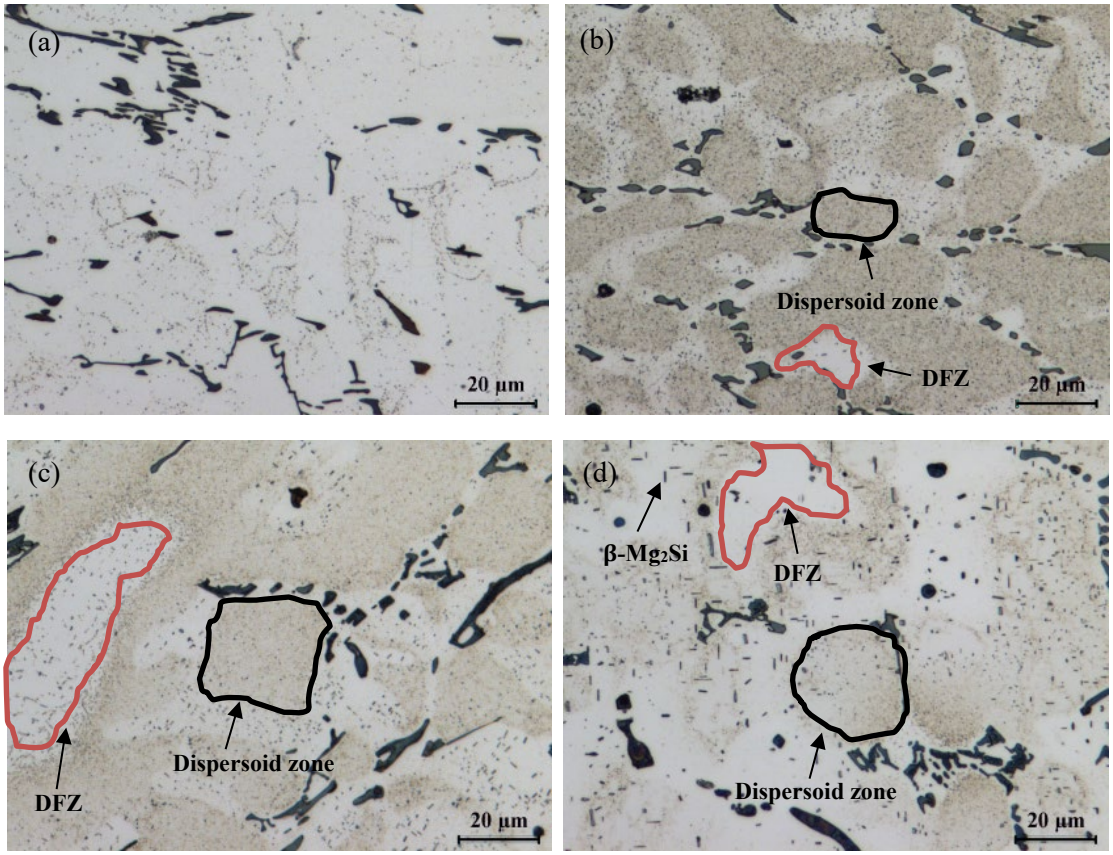

Fig. 4 Distribution of the dispersoid zone and DFZ in the DS series (a) DS0 alloy (0% Si), (b) DS25 alloy (0.23% Si), (c) DS45 alloy (0.42%Si) and (d) DS100 alloy (0.97% Si).

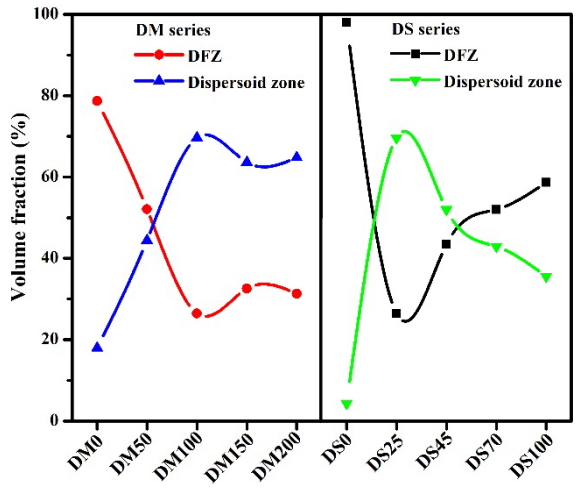

Fig. 5 Volume fraction of the dispersoid zone and DFZ in the DM and DS alloy series.

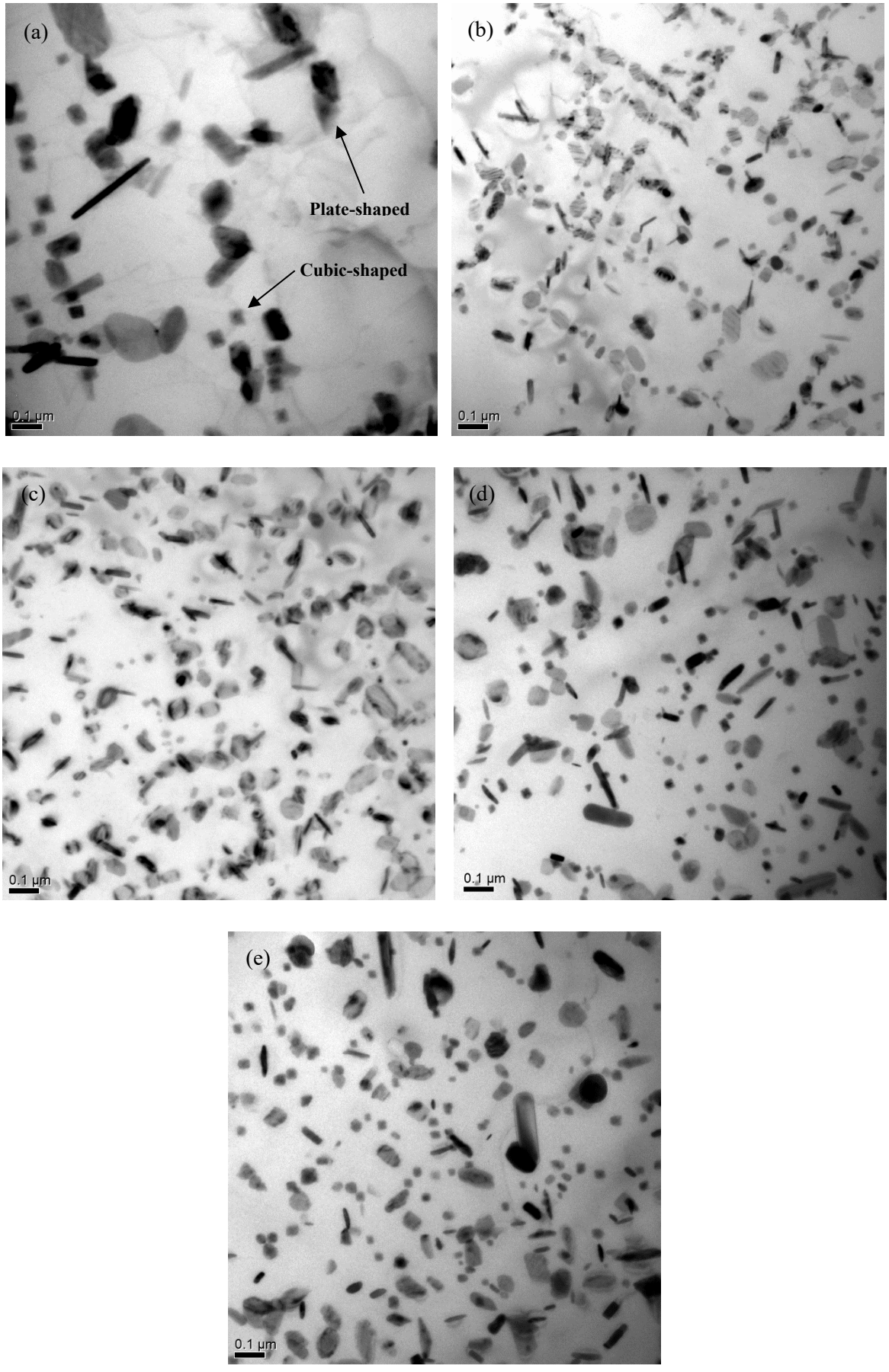
(a)
Plate-shaped
Cubic-shaped
0.1 μm
(b)
0.1 μm
(c)
0.1 μm
(d)
0.1 μm
(e)
0.1 μm

Fig.6 TEM images of dispersoid distribution in the DM series: (a) DM0 (0% Mg), (b) DM50 (0.47%% Mg), (c) DM100 (1.00% Mg), (d) DM150 (1.50% Mg) and (e) DM200 (2.02% Mg).

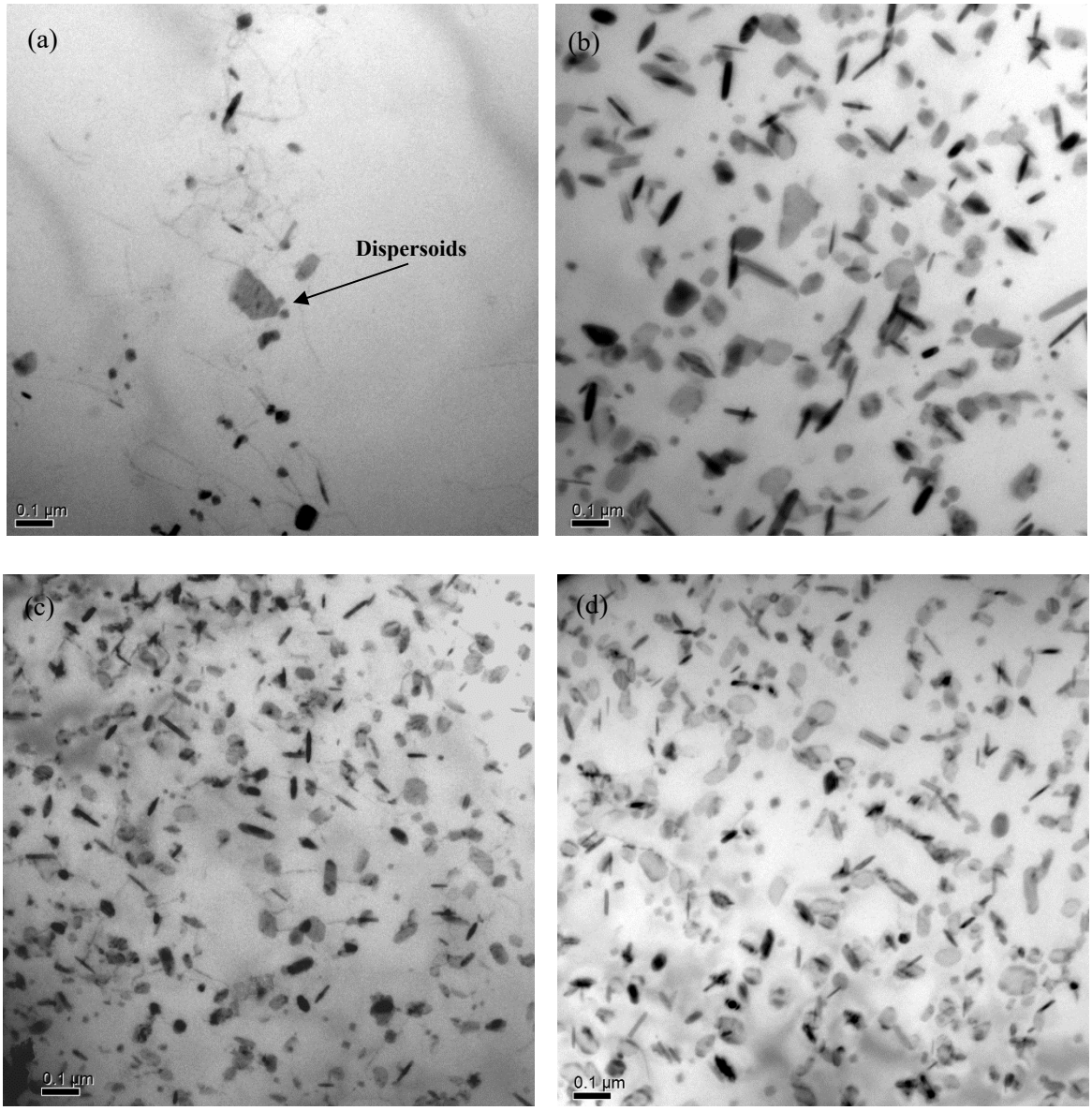

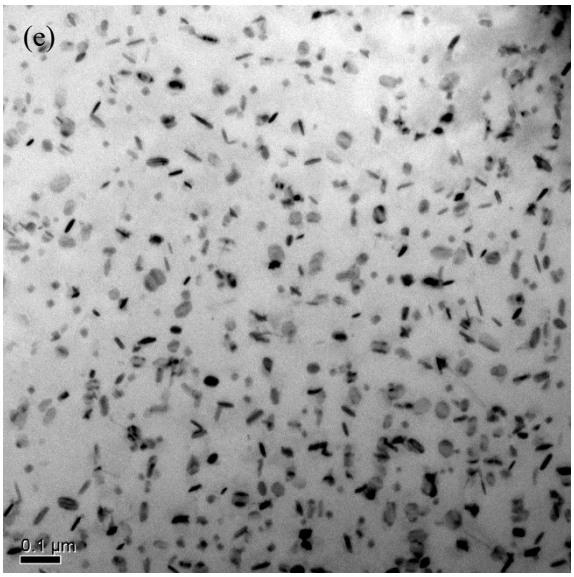

Fig.7 TEM images of dispersoid distribution in the DS series: (a) DS0 (0% Si), (b) DS25 alloy (0.23% Si), (c) DS45 (0.42% Si), (d) DS70 (0.70%) and (e) DS100 (0.97%Si).

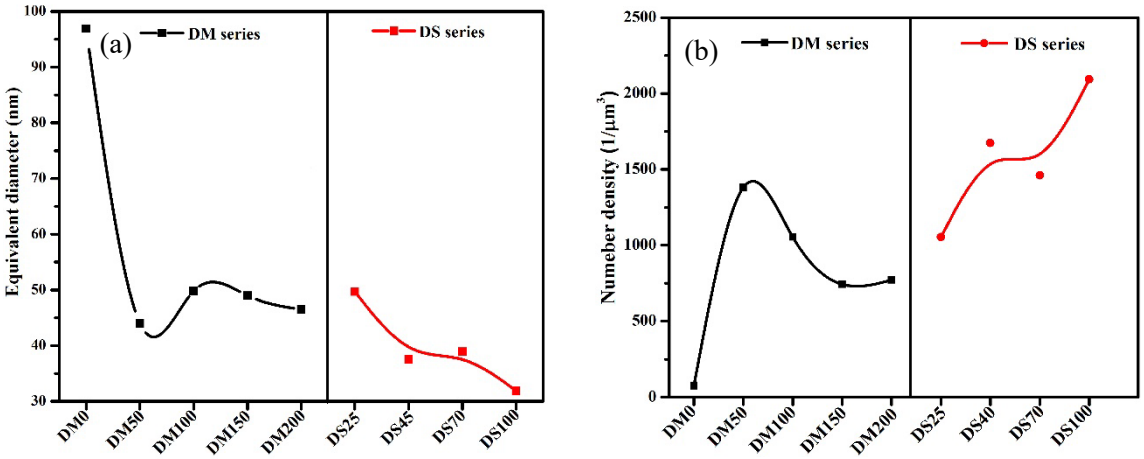

Fig. 8 Equivalent diameter (a) and number density (b) of disperoids in the DM and DS series.

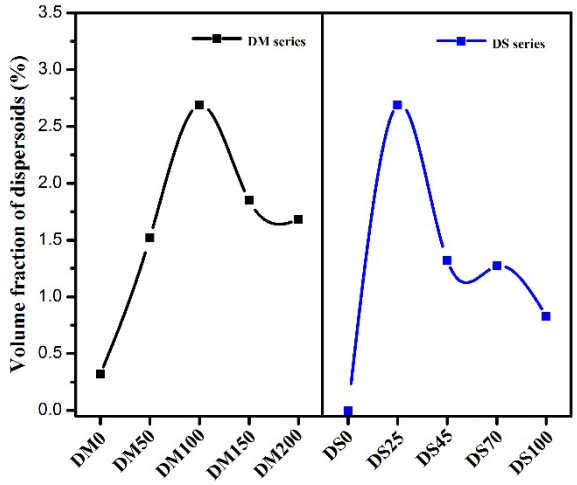

Fig. 9 Volume fraction of dispersoids in the DM and DS series.

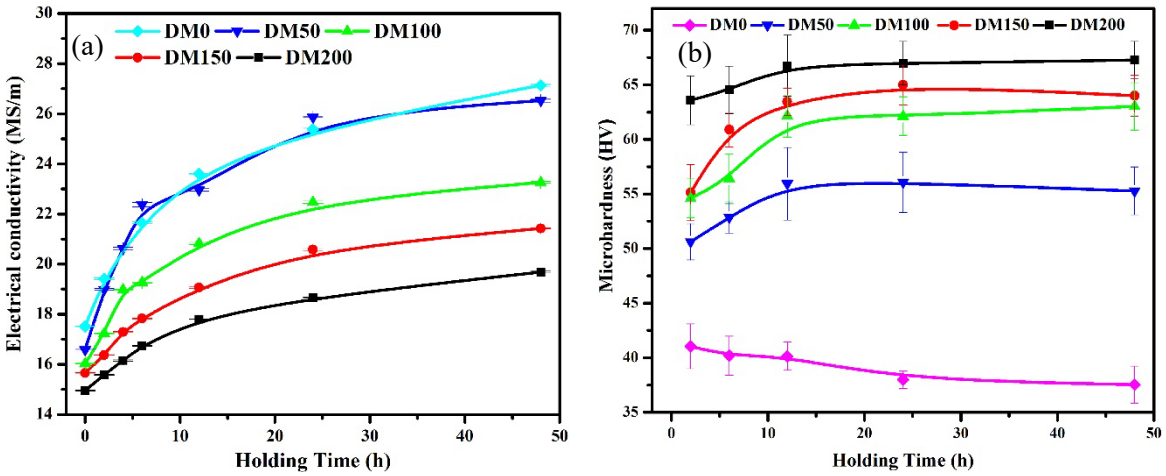

Fig. 10 Electrical conductivity (a) and microharness (b) as a function of holding time at 375 ℃ in the DM series.

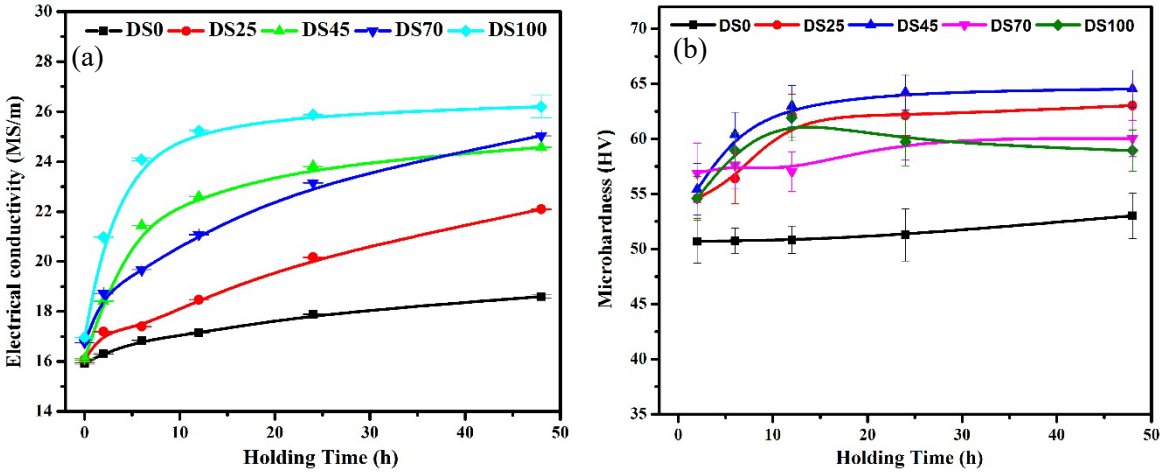

Fig. 11 Electrical conductivity (a) and microharness (b) as a function of holding time at 375 ℃ in the DS series.

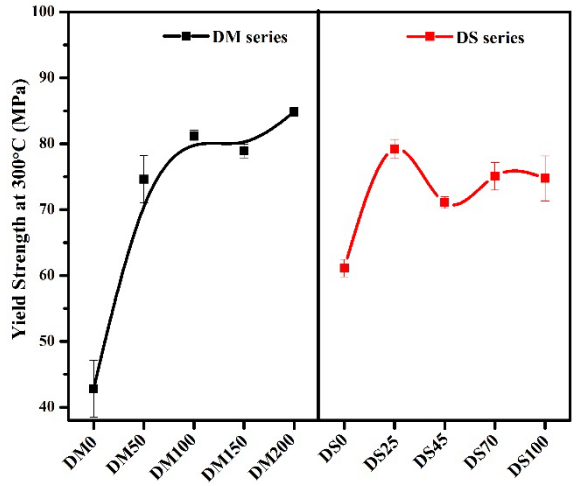

Fig. 12 Evolution of yield strength measured at 300 ℃ in the DM and DS series.

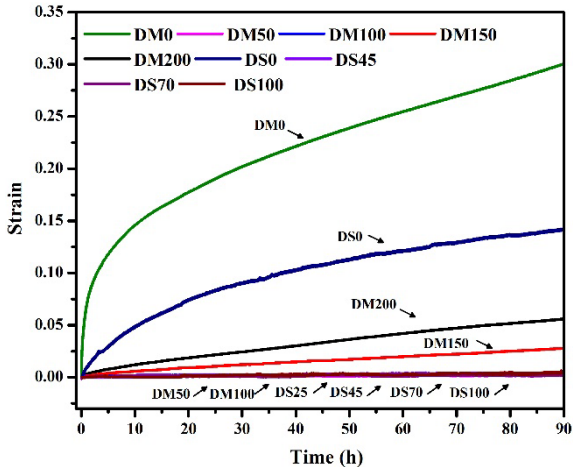

Fig. 13 Typical creep curves in the DM and DS series.

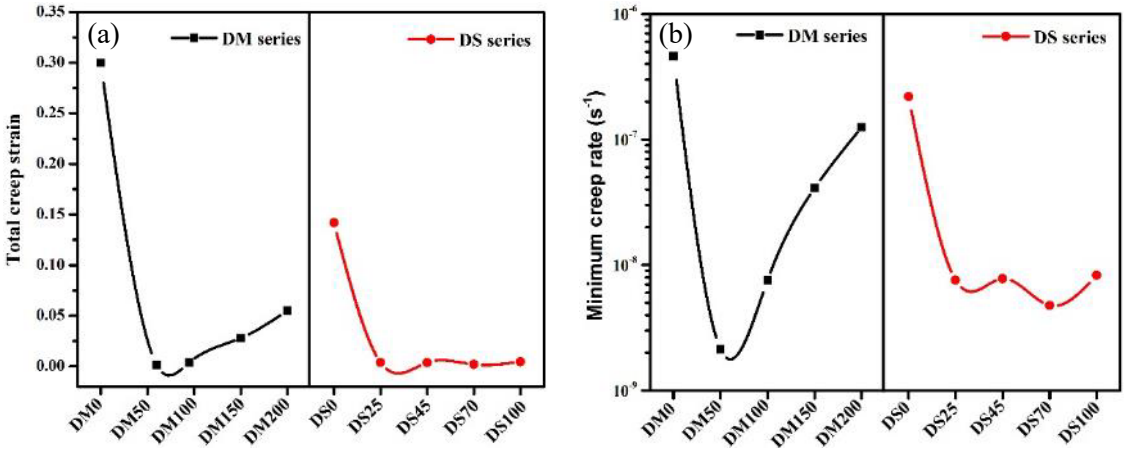

Fig.14 Total creep strain (a) and the minimum creep rate (b) of different alloys in the DM and DS series.

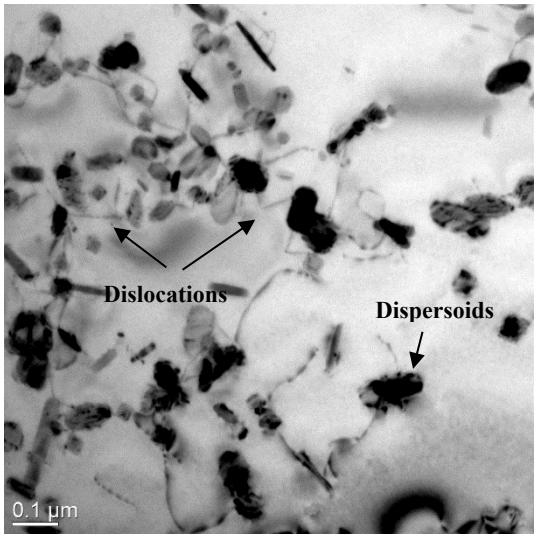

Fig. 15 TEM image of DM100 alloy after the creep test demonstrating the pinning effect of dispersoids on dislocations.

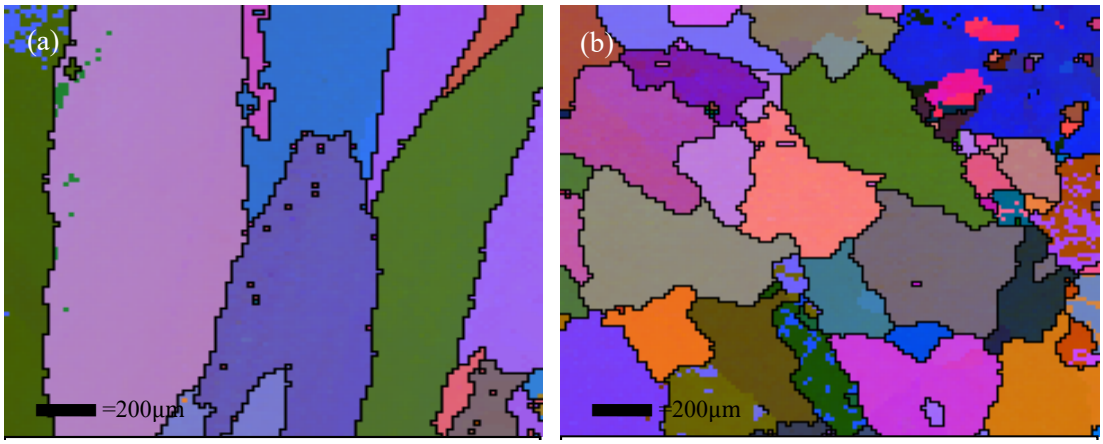

Fig. 16 EBSD images of grain structure (a) DM50 alloys (0.47%Mg) and (b) DM200 alloys (2.02%Mg) in as-cast condition.

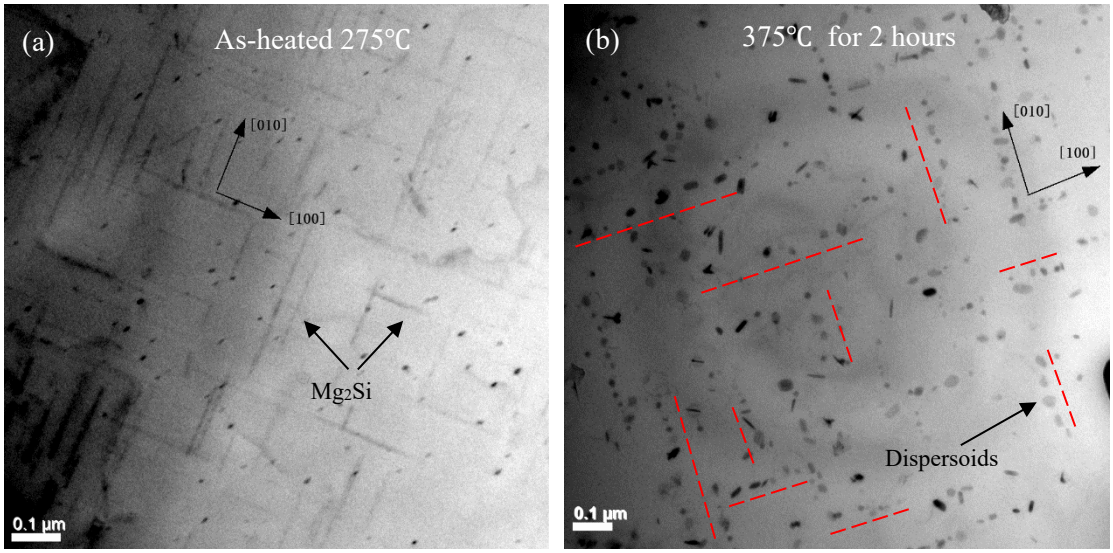

Fig. 17 TEM images of the water-quenched DM100 sample: (a) after heating to 275 ℃ and (b) after heat-treated at 375℃/2h. The red dash lines in (b) indicate the $<001>_{Al}$ direction.